

# REDUCED-ORDER MODELLING OF UNSTEADY SMALL-DISTURBANCE FLOWS USING A FREQUENCY-DOMAIN PROPER ORTHOGONAL DECOMPOSITION TECHNIQUE

Kenneth C. Hall<sup>\*</sup>, Jeffrey P. Thomas<sup>†</sup>, and Earl H. Dowell<sup>‡</sup>  
 Duke University  
 Durham, NC 27708-0300

## Abstract

A new method for constructing reduced-order models (ROM) of unsteady small-disturbance flows is presented. The reduced-order models are constructed using basis vectors determined from the proper orthogonal decomposition (POD) of an ensemble of small-disturbance frequency-domain solutions. Each of the individual frequency-domain solutions is computed using an efficient time-linearized flow solver. We show that reduced-order models can be constructed using just a handful of POD basis vectors, producing low-order but highly accurate models of the unsteady flow over a wide range of frequencies. In this paper, we apply the POD/ROM technique to compute the unsteady aerodynamic and aeroelastic behavior of an isolated transonic airfoil, and to a two-dimensional cascade of airfoils.

## Nomenclature

**A** = matrix defining homogeneous part of discretized aerodynamic operator  
 **$\mathcal{A}$**  = reduced-order form of **A**.  
 **$b$**  = airfoil semi-chord  
 **$\mathbf{b}$**  = vector defining inhomogeneous part of discretized aerodynamic operator  
 **$\mathbf{B}_0, \mathbf{B}_1$**  = matrices relating airfoil motion  **$\mathbf{h}$**  and  **$\dot{\mathbf{h}}$**  to  **$\mathbf{b}$**   
 **$c$**  = airfoil chord  
 **$\mathbf{C}$**  = matrix relating small-disturbance solution  **$\mathbf{q}$**  to aerodynamic force  **$\mathbf{f}$**   
 **$\hat{e}$**  = specific internal energy  
 **$\mathbf{f}$**  = vector of aerodynamic forces acting on airfoil  
 **$\mathbf{F}, \mathbf{G}$**  =  $x$  and  $y$  flux vectors  
 **$G$**  = cascade gap-to-chord ratio  
 **$h$**  = airfoil typical section plunging degree of freedom  
 **$\hat{h}$**  = specific enthalpy  
 **$\mathbf{h}$**  = vector of airfoil displacements  
 **$I_\alpha$**  = moment of inertia of airfoil section  
 **$\mathbf{I}$**  = identity matrix  
 **$j$**  =  $\sqrt{-1}$   
 **$J$**  = number of cells in computational grid  
 **$K$**  = number of POD vectors in reduced-order model

**$k_\alpha$**  = torsional stiffness of typical section  
 **$k_h$**  = bending stiffness of typical section  
 **$\mathbf{K}$**  = stiffness matrix of typical section model  
 **$L$**  = sectional airfoil lift  
 **$m$**  = mass of airfoil section  
 **$M$**  = number of solution snapshots; also Mach number  
 **$M_\alpha$**  = aerodynamic pitching moment  
 **$\mathbf{M}$**  = mass matrix of typical section model  
 **$N$**  = number of degrees of freedom in CFD model  
 **$\mathbf{N}$**  = vector operator defined by small-disturbance CFD model  
 **$\hat{p}$**  = static pressure  
 **$\mathbf{q}$**  = vector containing small-disturbance flow solution  
 **$r$**  = magnitude of Laplace variable  $s$   
 **$\mathbf{Q}$**  = vector containing steady flow solution  
 **$\mathbf{R}$**  = nonlinear vector operator defined by steady CFD model  
 **$s$**  = Laplace variable,  $s = j\omega$   
 **$S_\alpha$**  = static imbalance of airfoil typical section  
 **$\mathbf{S}$**  = matrix containing solution snapshots  
 **$t$**  = time  
 **$\hat{u}, \hat{v}$**  =  $x$  and  $y$ -components of velocity  
 **$\hat{\mathbf{u}}$**  = vector of unsteady nonlinear conservation variables  
 **$\mathbf{u}$**  = vector of unsteady small-disturbance conservation variables  
 **$\mathbf{U}$**  = vector of steady conservation variables  
 **$\mathbf{v}$**  = POD eigenvector  
 **$x, y$**  = Cartesian coordinates  
 **$\alpha$**  = airfoil typical section pitching degree of freedom  
 **$\gamma$**  = ratio of specific heats  
 **$\theta$**  = angle made by Laplace variable  $s$  in complex plane,  $s = re^{j\theta}$   
 **$\Theta$**  = cascade stagger angle  
 **$\lambda$**  = POD eigenvalue  
 **$\mu$**  = mass ratio,  $\mu = m/(\pi\rho b^2)$   
 **$\xi$**  = aerodynamic state variable  
 **$\boldsymbol{\xi}$**  = vector of aerodynamic state variables  
 **$\Pi$**  = quantity extremized to find POD vectors  
 **$\hat{\rho}$**  = static density  
 **$\sigma$**  = interblade phase angle of cascade vibration  
 **$\phi$**  = POD vector  
 **$\Phi$**  = matrix of POD vectors  
 **$\omega$**  = frequency

**Subscripts**  
 $\infty$  = freestream conditions

<sup>\*</sup>Associate Professor, Department of Mechanical Engineering and Materials Science, Associate Fellow AIAA.

<sup>†</sup>Research Assistant Professor, Department of Mechanical Engineering and Materials Science, Member AIAA.

<sup>‡</sup>Professor, Department of Mechanical Engineering and Materials Science, and Dean, School of Engineering, Fellow AIAA.

Copyright © 1999 by Kenneth C. Hall, Jeffrey P. Thomas, and Earl H. Dowell. Published by the American Institute of Aeronautics and Astronautics, Inc. with permission.

## I. Introduction

Unsteady aerodynamic theories and computational fluid dynamic (CFD) models for the computation of unsteady flows about airfoils, wings, and turbomachinery cascades are quite complex, even for relatively simple flow models. Furthermore, the forms of these analytical and computational flow models, most often cast in the time or frequency domain, are not well suited for the direct computation of aeroelastic stability – nor are they well suited for applications involving active control. Analytical models are usually formulated in the frequency domain for real frequencies and, therefore, the aerodynamic transfer function is not composed of simple poles and zeros. For example, the Theodorsen function has a branch cut with a branch point at the origin of the Laplace plane. Computational fluid dynamic models, on the other hand, may have many thousands of degrees of freedom, making them unwieldy for aeroelastic stability and control computations.

Investigators have developed a number of techniques to reduce the complexity of unsteady aerodynamic models. R. T. Jones [1] approximated indicial lift functions with series of exponentials in time. Such series have particularly simple Laplace transforms, i.e. rational polynomials in the Laplace variable  $s$ , making them especially useful for aeroelastic computations. Padé approximants are rational polynomials whose coefficients are found by least-squares curve fitting the computed aerodynamic loads computed over a range of frequencies. Vepa [2], Edwards [3], and Karpel [4] developed various forms of the matrix Padé approximant technique. This approach reduces the number of so-called augmented states needed to model the various unsteady aerodynamic transfer functions (lift due to pitching, pitching moment due to pitching, etc.) by requiring that all the transfer functions share common poles.

Hall [5], Hall et al. [6], Florea & Hall [7], and Romanowski & Dowell [8] have developed reduced-order unsteady aerodynamic models of flows about airfoils, wings, and turbomachinery cascades. Using this approach, the dominant eigenvalues and eigenmodes of a time-domain or frequency-domain CFD model of unsteady flow are computed. The eigenmodes are then used as basis vectors for the construction of reduced-order models. This eigenmode reduction technique works well provided one or multiple static corrections are applied to account for the eigenmodes not retained in the reduced-order model. For a review of the eigenmode reduction technique, see Dowell et al. [9]

More recently, a number of researchers have used the proper orthogonal decomposition (POD) technique, also known as Karhunen-Loève [10] expansions, to determine and model coherent structures in turbulent flow fields. Lumley [11] was the first to propose using proper orthogonal decomposition to uncover coherent structures in turbulent flow fields. Using this approach, one examines a series of “snapshots” of experimental or computational data, each at a different instant in time. These solution snapshots are used to form a small eigenvalue problem that is solved to determine a set of optimal basis functions for representing the flow field. Other examples include work by Berkooz et al. [12], Poje & Lumley [13], Sirovich [14, 15, 16], Moin & Moser [17], Rempfer and Fasel [18, 19], and Deane et

al. [20]. A recently published book by Holmes et al. [21] provides an overview of the POD method along with extensive details of how the method has been used by researchers to study a wide variety of fluids problems.

A number of researchers have used the time-domain POD technique to construct reduced-order models (ROM) of unsteady aerodynamic flows. Romanowski [22], for example, has used the POD technique to create a reduced-order aeroelastic model of a two-dimensional isolated airfoil, including compressible aerodynamics. Romanowski has shown that very accurate unsteady flow models can be constructed that reduce the number of degrees of freedom from the thousands associated with the original CFD flow solver to a few tens of degrees of freedom. Tang et al. [23] have used the POD technique to create a reduced order model of vortex shedding from a cylinder. They proposed that the reduced-order model could then be used to design an active control system to control the shedding.

Most of the previous work using proper orthogonal decomposition has used data sampled from the time domain, or from ensembles of steady data as in the case of graphical feature recognition. Recently, however, Kim [24] has developed a frequency domain form. Using this approach, snapshots of the unsteady flow are computed at a number of discrete frequencies rather than at discrete instants in time. He applied the technique to two relatively simple dynamic systems – a 12 degree-of-freedom mass-spring damper system, and an incompressible three-dimensional vortex lattice model of a rectangular wing.

In this paper, we develop a frequency-domain form of the POD technique. Here, we use a time-linearized CFD analysis to compute unsteady small-disturbance flow solutions for vibrating airfoils in the frequency domain over a range of frequencies. Basis vectors are then extracted from this frequency-domain data set using the POD technique. The resulting basis vectors are then used to construct low degree of freedom reduced-order models of the unsteady flow. Finally, the reduced-order aerodynamic model are combined with a structural dynamic model resulting in a compact, but accurate, flutter model. In this paper, we apply the technique to a two-dimensional transonic airfoil, and also to a two-dimensional cascade of vibrating airfoils. Although the results presented here are two-dimensional, the method itself is general, and can be readily extended to three-dimensional flow problems.

## II. Theory

### A. Steady and Small-Disturbance Unsteady Flow Models

Although the proper orthogonal decomposition technique may be applied to a wide range of linear and nonlinear flow problems, in this paper we consider only small-disturbance unsteady two-dimensional inviscid flows. Thus, we consider the time-dependent two-dimensional Euler equations, which may be expressed as

$$\frac{\partial \hat{\mathbf{u}}}{\partial t} + \frac{\partial \mathbf{F}(\hat{\mathbf{u}})}{\partial x} + \frac{\partial \mathbf{G}(\hat{\mathbf{u}})}{\partial y} = \mathbf{0} \quad (1)$$

where  $x$  and  $y$  are the Cartesian coordinates,  $t$  is time, and  $\hat{\mathbf{u}}$  is the vector of conservation variables given by

$$\hat{\mathbf{u}}(x, y, t) = \begin{Bmatrix} \hat{\rho} \\ \hat{\rho}\hat{u} \\ \hat{\rho}\hat{v} \\ \hat{\rho}\hat{e} \end{Bmatrix} \quad (2)$$

and  $\hat{\rho}$ ,  $\hat{u}$ ,  $\hat{v}$ , and  $\hat{e}$  are the static density,  $x$ - and  $y$ -components of velocity, and total specific energy, respectively. The flux vectors  $\mathbf{F}$  and  $\mathbf{G}$  are given by

$$\mathbf{F}(\hat{\mathbf{u}}) = \begin{Bmatrix} \hat{\rho}\hat{u} \\ \hat{\rho}\hat{u}^2 + \hat{p} \\ \hat{\rho}\hat{u}\hat{v} \\ \hat{\rho}\hat{u}\hat{h} \end{Bmatrix}, \quad \mathbf{G}(\hat{\mathbf{u}}) = \begin{Bmatrix} \hat{\rho}\hat{v} \\ \hat{\rho}\hat{u}\hat{v} \\ \hat{\rho}\hat{v}^2 + \hat{p} \\ \hat{\rho}\hat{v}\hat{h} \end{Bmatrix} \quad (3)$$

where the specific enthalpy  $\hat{h}$  is

$$\hat{h} = \frac{\hat{\rho}\hat{e} + \hat{p}}{\hat{\rho}} \quad (4)$$

and, for a calorically perfect gas, the pressure  $\hat{p}$  is given by

$$\hat{p} = (\gamma - 1) \left[ \hat{\rho}\hat{e} - \frac{\hat{\rho}}{2} (\hat{u}^2 + \hat{v}^2) \right] \quad (5)$$

In the present investigation, we are interested in small-disturbance, harmonically varying unsteady flows about some nonlinear mean operating condition. Thus, we assume the conservative variables  $\hat{\mathbf{u}}$  may be expanded in a perturbation series of the form

$$\hat{\mathbf{u}}(x, y, t) = \mathbf{U}(x, y) + \mathbf{u}(x, y)e^{j\omega t} \quad (6)$$

where  $\mathbf{U}(x, y)$  represents for a given problem the steady background flow, which is also a solution to Eq. (1). Also,  $\mathbf{u}(x, y)$  is the complex amplitude of the small-disturbance unsteady flow that arises from an external excitation with frequency  $\omega$ .

Substituting Eq. (6) into the nonlinear Euler equations, Eq. (1), and expanding the result in a perturbation series in the small-disturbance quantities, one finds that to zeroth order, the governing equations are given by

$$\frac{\partial \mathbf{F}(\mathbf{U})}{\partial x} + \frac{\partial \mathbf{G}(\mathbf{U})}{\partial y} = \mathbf{0} \quad (7)$$

This vector equation is just the steady Euler equations that describes the steady background flow. The first-order equation describes the small-disturbance unsteady flow, and is given by

$$j\omega \mathbf{u} + \frac{\partial}{\partial x} \left( \frac{\partial \mathbf{F}}{\partial \mathbf{U}} \mathbf{u} \right) + \frac{\partial}{\partial y} \left( \frac{\partial \mathbf{G}}{\partial \mathbf{U}} \mathbf{u} \right) = \mathbf{0} \quad (8)$$

where, for example,

$$\frac{\partial \mathbf{F}}{\partial \mathbf{U}} = \left. \frac{\partial \mathbf{F}(\hat{\mathbf{u}})}{\partial \hat{\mathbf{u}}} \right|_{\hat{\mathbf{u}}=\mathbf{U}} \quad (9)$$

Equations (7) and (8) are solved sequentially, with boundary conditions that depend on the particular physical problem to be solved.

## B. Numerical Discretization Scheme

The starting point for the construction of a POD based reduced order model is a conventional CFD scheme. In this study, we use a time-linearized (i.e. frequency domain) small-disturbance flow solver.

The steady and time-linearized flow equations are discretized on a computational mesh composed of quadrilateral cells. At the center of the  $j$ th cell of the computational grid, the estimate of the solution  $\mathbf{u}$  is stored, and is denoted by  $\mathbf{u}_j$ . The steady and unsteady solution for the entire computational domain may be thought of as vectors of the form

$$\mathbf{q} = \begin{Bmatrix} \mathbf{u}_1 \\ \mathbf{u}_2 \\ \vdots \\ \mathbf{u}_J \end{Bmatrix} \quad \text{and} \quad \mathbf{Q} = \begin{Bmatrix} \mathbf{U}_1 \\ \mathbf{U}_2 \\ \vdots \\ \mathbf{U}_J \end{Bmatrix} \quad (10)$$

where  $J$  is the total number of computational cells. Thus, the total number of entries  $N$  in each of the two vectors in Eq. (10) is  $N = 4 \times J$ .

Next, the steady and time-linearized Euler equations are discretized. In this study, we use a second-order, explicit, finite-volume Godunov [25] method using Roe's [26] approximate Riemann solver with van Leer's [27] technique for preserving monotonicity and better than first-order accuracy. The resulting discretization of the steady Euler equations can be expressed as

$$\mathbf{Q}^{n+1} - \mathbf{Q}^n = \mathbf{R}(\mathbf{Q}^n) \quad (11)$$

where  $n$  is the iteration number. To solve for the steady flow, the solution is advanced in time until a steady-state solution is obtained.

Similarly, once the steady flow has been computed, the time-linearized unsteady Euler equations are discretized with the result

$$\mathbf{q}^{n+1} - \mathbf{q}^n = \mathbf{N}(\mathbf{q}^n; \mathbf{Q}, \omega, \Delta) \quad (12)$$

where  $\Delta$  is a shorthand notation for the particular type of external source of excitation. Note the boundary conditions themselves may be functions of  $\omega$ . In other words, the unsteady flow depends on the steady flow, the frequency of the disturbance, and the type of excitation.

Although  $\mathbf{N}$  is an operator for solving a time-linearized system of equations,  $\mathbf{N}$  is not – strictly speaking – a linear operator because of the presence of inhomogeneous boundary conditions (i.e.  $\mathbf{N}(\mathbf{0}) \neq \mathbf{0}$ ). Nevertheless, the operator  $\mathbf{N}$  may be expressed as a linear system of equations of the form

$$\mathbf{N}(\mathbf{q}; \omega, \Delta) = [\mathbf{A}(\omega)]\mathbf{q} - \mathbf{b}(\omega, \Delta) = \mathbf{0} \quad (13)$$

where  $\mathbf{A}$  is a large sparse matrix and  $\mathbf{b}$  is a vector arising from the imposition of unsteady inhomogeneous boundary conditions.

For our discretization scheme, the matrix  $\mathbf{A}$  and the vector  $\mathbf{b}$  are first order in  $\omega$ . Thus, Eq. (13) can be written as

$$[\mathbf{A}_0]\{\mathbf{q}\} + j\omega[\mathbf{A}_1]\{\mathbf{q}\} = \mathbf{b}_0 + j\omega\mathbf{b}_1 \quad (14)$$

where  $\mathbf{A}_0$  and  $\mathbf{A}_1$  are independent of the excitation frequency  $\omega$ . For unsteady flows about isolated airfoils, the

matrices  $\mathbf{A}_0$  and  $\mathbf{A}_1$  are purely real. For unsteady flows about a cascade of airfoils, the matrices may be complex due to the complex periodic boundary conditions used to impose the fixed interblade phase angle  $\sigma$  of a travelling wave disturbance.

In some instances, one would like to compute the homogeneous solutions of the discretized unsteady aerodynamic model. Such would be the case, for example, if one wanted to compute the onset of vortex shedding for an airfoil, or rotating stall for a turbomachinery compressor. Setting the right-hand side of Eq. (14) to zero, one obtains the eigenvalue problem

$$[\mathbf{A}_0]\{\mathbf{q}\} + s[\mathbf{A}_1]\{\mathbf{q}\} = \mathbf{0} \quad (15)$$

where the eigenvalue  $s = j\omega$  will, in general, be complex, as will the eigenvectors. For the isolated airfoil case, the complex eigenvalues (and corresponding eigenvectors) will appear in complex conjugate pairs. One should be careful when interpreting the eigenvalues of the CFD model. Some of the eigenvalues will be (nearly) equal to the eigenvalues of the physical system. Others, however, form a discrete approximation of a branch cut in the Laplace plane (see Hall [5]).

### C. Definition of POD Basis Vectors

The idea behind the frequency-domain proper orthogonal decomposition technique is a simple one. We first calculate the small-disturbance response of the aerodynamic system at  $M$  different combinations of frequency and excitation. The solutions (also called ‘‘snapshots’’) are denoted by  $\mathbf{q}^m$  for  $m = 1, 2, \dots, M$ . These snapshots are then linearly combined to form a smaller number of basis vectors  $\phi_k$  for  $k = 1, 2, \dots, K$  where  $K < M$ . In other words,

$$\phi_k = \sum_{m=1}^M \mathbf{q}^m v_k^m, \quad k = 1, 2, 3, \dots, K \quad (16)$$

where  $v_k^m$  is the contribution of the  $m$ th snapshot to the  $k$ th basis vector. In matrix form, Eq. (16) is written as

$$\phi_k = \mathbf{S} \mathbf{v}_k \quad (17)$$

where

$$\mathbf{S} = \begin{bmatrix} | & | & \dots & | \\ \mathbf{q}^1 & \mathbf{q}^2 & \dots & \mathbf{q}^M \\ | & | & \dots & | \end{bmatrix} \quad (18)$$

and

$$\mathbf{v}_k = \begin{Bmatrix} v_k^1 \\ v_k^2 \\ \vdots \\ v_k^M \end{Bmatrix} \quad (19)$$

We assume here the vector  $\mathbf{v}_k$  has been suitably scaled so that the vectors  $\phi_k$  are unit length. The vectors  $\mathbf{v}_k$  are selected so that they lie along the principal axes of the space spanned by  $\mathbf{S}$ , that is, the quantity

$$\| \mathbf{S}^H \mathbf{S} \mathbf{v}_k \|_2 \quad (20)$$

is extremized subject to the constraint that  $\phi_k$  is unit length. Thus, introducing the Lagrange multiplier  $\lambda_k$ , we find the vector  $\mathbf{v}_k$  that makes  $\Pi$  stationary, where

$$\Pi = \mathbf{v}_k \mathbf{S}^H \mathbf{S} \mathbf{S}^H \mathbf{S} \mathbf{v}_k - \lambda_k (\mathbf{v}_k \mathbf{S}^H \mathbf{S} \mathbf{v}_k - 1) \quad (21)$$

Taking the variation of  $\Pi$  and setting the result to zero gives

$$\mathbf{S}^H \mathbf{S} \mathbf{v}_k = \lambda_k \mathbf{v}_k \quad (22)$$

Equation (22) defines an eigenvalue problem for the eigenvectors  $\mathbf{v}_k$  and eigenvalues  $\lambda_k$ . Those eigenvectors with the largest values of  $\lambda_k$  give the largest values of the quantity in Eq. (19). Said another way, the snapshots  $\mathbf{q}^m$  tend to lie in a sub-space spanned by the basis vectors  $\phi_k$  with the largest eigenvalues  $\lambda_k$ .

### D. Reduced-Order Aerodynamic Model

Having computed the POD basis vectors, we assume that they will provide a useful basis for computing the unsteady solution at some other frequency and/or external excitation than was used to generate the original snapshots. Thus, we let

$$\mathbf{q} = \sum_{k=1}^K \phi_k \xi_k \quad (23)$$

where  $\xi_k$  may be thought of as an aerodynamic state variable (sometimes referred to as an augmented aerodynamic state in the Pad  literature). In matrix form, Eq. (23) is given by

$$\mathbf{q} = \Phi \boldsymbol{\xi} \quad (24)$$

where  $\Phi$  is an  $N \times K$  matrix whose  $k$ th column is simply the basis vector  $\phi_k$ , and  $\boldsymbol{\xi}$  is the vector of aerodynamic state variables. Substitution of Eq. (24) into Eq. (13) gives

$$\mathbf{A} \Phi \boldsymbol{\xi} = \mathbf{b} \quad (25)$$

In practice, the matrix  $\mathbf{A}$  is never actually computed. Instead, we compute the  $k$ th column of  $\mathbf{A} \Phi$  using the original linearized flow solver itself. That is,

$$\mathbf{A} \phi_k = \mathbf{N}(\phi_k) - \mathbf{N}(\mathbf{0}) \quad (26)$$

Next, we project the error in Eq. (25) onto the space spanned by the basis vectors to obtain

$$\Phi^H \mathbf{A} \Phi \boldsymbol{\xi} = \mathcal{A} \boldsymbol{\xi} = \Phi^H \mathbf{b} \quad (27)$$

Finally, the matrix  $\mathcal{A}$  is factored using LU decomposition, and Eq. (27) is solved for the unknown aerodynamic state variables  $\boldsymbol{\xi}$ . This step is computationally very efficient because the reduced-order matrix  $\mathcal{A}$  is quite small, sometimes as small as  $10 \times 10$ , but rarely larger than  $100 \times 100$ .

The major expense in constructing the aerodynamic reduced-order model is the computation of the snapshots; the computational cost of finding the basis vectors and solution to Eq. (27) is negligible by comparison.

The computational cost of computing even a few of the eigenvalues of the full CFD model of the unsteady flow (Eq. 15) can be quite large, especially for viscous and/or three-dimensional flow models. An alternative is to compute the eigenvalues with a Ritz approach, using the POD

modes as basis vectors. Recalling that the matrix  $\mathbf{A}$  is first order in  $\omega$ , the homogeneous part of Eq. (27) may be written as

$$\mathcal{A}_0 \boldsymbol{\xi} + s \mathcal{A}_1 \boldsymbol{\xi} = \mathbf{0} \quad (28)$$

where

$$\mathcal{A}_0 = \Phi^H \mathbf{A}_0 \Phi, \quad \mathcal{A}_1 = \Phi^H \mathbf{A}_1 \Phi \quad (29)$$

Equation (28) may be used to determine the dominant eigenvalues and eigenvectors of the full CFD model, but Eq. (28) has many fewer degrees of freedom than the original system, greatly reducing the computational cost.

### E. Reduced-Order Aeroelastic Model

Having described the basic reduced-order modelling technique, we next describe how to incorporate an aerodynamic reduced-order model into an aeroelastic model of flutter. Consider a two degree-of-freedom structural dynamic model of a typical section. The governing equations of motion are of the form

$$\mathbf{M} \ddot{\mathbf{h}} + \mathbf{K} \mathbf{h} = \mathbf{f} \quad (30)$$

where

$$\mathbf{h} = \begin{Bmatrix} h \\ \alpha \end{Bmatrix} \quad (31)$$

and  $h$  and  $\alpha$  are the plunging and pitching degrees of freedom of the typical section. Also,

$$\mathbf{M} = \begin{bmatrix} m & S_\alpha \\ S_\alpha & I_\alpha \end{bmatrix}, \quad \mathbf{K} = \begin{bmatrix} k_h & 0 \\ 0 & k_\alpha \end{bmatrix}, \quad \mathbf{f} = \begin{Bmatrix} -L \\ M_\alpha \end{Bmatrix} \quad (32)$$

where  $m$ ,  $S_\alpha$ , and  $I_\alpha$  are the mass, static imbalance, and moment of inertia of the airfoil section measured about the elastic axis,  $k_h$  and  $k_\alpha$  are the bending and torsional spring constants, and  $L$  and  $M_\alpha$  are the aerodynamic lift and moment produced by the motion of the airfoil.

Note that the aerodynamic force vector  $\mathbf{f}$  is obtained from integrals involving the pressure at the surface of the airfoil. When discretized, these integrals may be expressed as

$$\mathbf{f} = \mathbf{C} \mathbf{q} \quad (33)$$

where  $\mathbf{C}$  is a sparse  $2 \times N$  matrix. Similarly, for the case of airfoil vibration, the vector  $\mathbf{b}$  on the right-hand side of Eq. (14) can be expressed as

$$\mathbf{b} = \mathbf{b}_0 + j\omega \mathbf{b}_1 = \mathbf{B}_0 \mathbf{h} + j\omega \mathbf{B}_1 \mathbf{h} \quad (34)$$

where now we have made the assumption that the airfoil motion is harmonic in time, i.e.  $\mathbf{h} = \hat{\mathbf{h}} \exp(j\omega t)$  ( $\omega$  may be complex). Putting together Eq. (14) and Eqs. (30)–(34), and converting to first order in  $\omega$  (state-space form) gives

$$\begin{bmatrix} \mathbf{A}_0 & -\mathbf{B}_0 & -\mathbf{B}_1 \\ \mathbf{0} & \mathbf{0} & \mathbf{I} \\ -\mathbf{C} & \mathbf{K} & \mathbf{0} \end{bmatrix} \begin{Bmatrix} \mathbf{q} \\ \mathbf{h} \\ \dot{\mathbf{h}} \end{Bmatrix} + j\omega \begin{bmatrix} \mathbf{A}_1 & \mathbf{0} & \mathbf{0} \\ \mathbf{0} & -\mathbf{I} & \mathbf{0} \\ \mathbf{0} & \mathbf{0} & \mathbf{M} \end{bmatrix} \begin{Bmatrix} \mathbf{q} \\ \mathbf{h} \\ \dot{\mathbf{h}} \end{Bmatrix} = \mathbf{0} \quad (35)$$

Equation (35) is a large sparse  $(N+4) \times (N+4)$  generalized eigenvalue problem that describes the aeroelastic stability of the airfoil.

For large CFD models, finding the eigenvalues of Eq. (35) is prohibitively expensive. To reduce the size of the model, we again assume that the number of aerodynamic states can be reduced using Eq. (24), so that

$$\begin{bmatrix} \mathbf{A}_0 \Phi & -\mathbf{B}_0 & -\mathbf{B}_1 \\ \mathbf{0} & \mathbf{0} & \mathbf{I} \\ -\mathbf{C} \Phi & \mathbf{K} & \mathbf{0} \end{bmatrix} \begin{Bmatrix} \boldsymbol{\xi} \\ \mathbf{h} \\ \dot{\mathbf{h}} \end{Bmatrix} + j\omega \begin{bmatrix} \mathbf{A}_1 \Phi & \mathbf{0} & \mathbf{0} \\ \mathbf{0} & -\mathbf{I} & \mathbf{0} \\ \mathbf{0} & \mathbf{0} & \mathbf{M} \end{bmatrix} \begin{Bmatrix} \boldsymbol{\xi} \\ \mathbf{h} \\ \dot{\mathbf{h}} \end{Bmatrix} = \mathbf{0} \quad (36)$$

Finally, projecting the error in the aerodynamic equations onto the space spanned by the basis vectors gives

$$\begin{bmatrix} \mathcal{A}_0 & -\Phi^H \mathbf{B}_0 & -\Phi^H \mathbf{B}_1 \\ \mathbf{0} & \mathbf{0} & \mathbf{I} \\ -\mathbf{C} \Phi & \mathbf{K} & \mathbf{0} \end{bmatrix} \begin{Bmatrix} \boldsymbol{\xi} \\ \mathbf{h} \\ \dot{\mathbf{h}} \end{Bmatrix} + j\omega \begin{bmatrix} \mathcal{A}_1 & \mathbf{0} & \mathbf{0} \\ \mathbf{0} & -\mathbf{I} & \mathbf{0} \\ \mathbf{0} & \mathbf{0} & \mathbf{M} \end{bmatrix} \begin{Bmatrix} \boldsymbol{\xi} \\ \mathbf{h} \\ \dot{\mathbf{h}} \end{Bmatrix} = \mathbf{0} \quad (37)$$

Equation (37) is the reduced-order aeroelastic model, which is a generalized eigenvalue problem of size  $(K+4) \times (K+4)$ , where  $K \ll N$ .

Equation (37) is similar in form to that obtained using a matrix Padé approximant for the unsteady aerodynamics (see e.g. Karpel [4]), and has some of the same advantages of the Padé approach. Both methods produce low degree-of-freedom models. Furthermore, both require the aerodynamic lift and moment transfer functions to share common eigenvalues (although the zeros are obviously different). This is appealing because physically the poles should be independent of the type of transfer function. However, the present approach has several advantages over the matrix Padé approximant method. The present method attempts to compute the actual aerodynamic poles, or at least the poles of a rational CFD model. The Padé approach, on the other hand, selects pole locations by some form of curve fitting. In fact, some Padé techniques can produce unstable aerodynamic poles, even for stable aerodynamic systems.

## III. Computational Results

### A. Ames NACA 64A010 Airfoil

In this section, we present some typical two-dimensional steady and unsteady small-disturbance flow solutions for a simple model problem. The results presented are based on a standard aeroelastic test case proposed by AGARD to test the ability of computational methods to predict flutter of aircraft wings [28]. The airfoil used closely approximates a NACA 64A010 airfoil, but it is slightly asymmetric and 10.6 percent thick; this airfoil was experimentally studied at NASA Ames Research Center. For the results presented here, we used two computational grids, one fine grid containing  $128 \times 32$  computational cells, and one coarse grid with  $32 \times 16$  cells. The fine grid is shown in Figure 1.

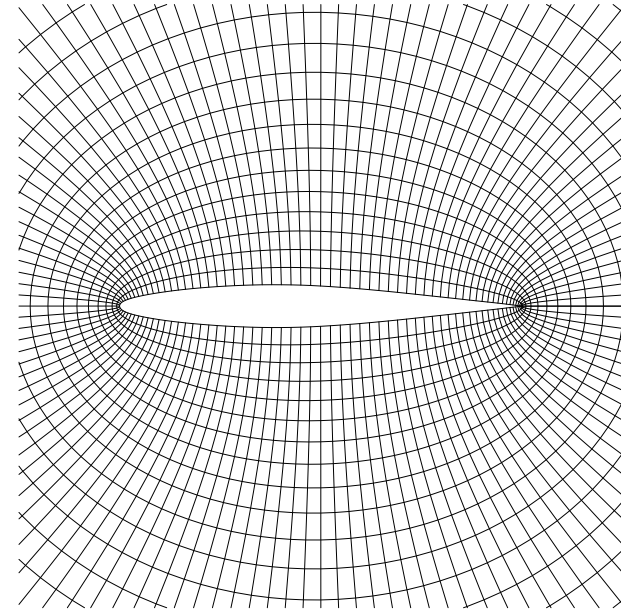
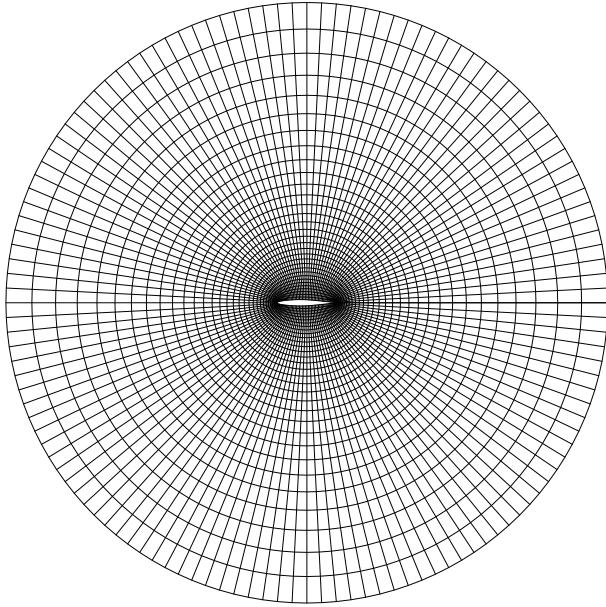


**Figure 1: Computational grid for Ames NACA 64A010 airfoil. Top: full grid. Bottom: grid near airfoil.**

Shown in Fig. 2 are the computed steady pressure distributions for several inflow Mach numbers at zero angle of attack. These solutions were computed on the fine computational grid. Note that the solutions are slightly asymmetric due to the slight asymmetry in the airfoil shape. As the Mach number is increased, shocks form on the pressure and suction surfaces of the airfoil; these shocks move aft as the Mach number is increased. One observes that the solution is somewhat “wavy” near the leading edge of the airfoil. The authors believe this is a result of the coarse airfoil definition; only 96 surface points were provided in the original AGARD report. The problem is accentuated by the use of splines to interpolate the data when generating the computational grid.

Having computed the steady flow, we next consider the

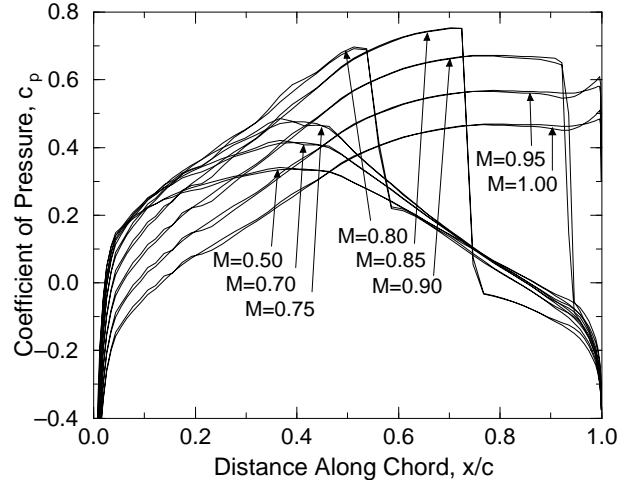


**Figure 2: Steady surface pressure distributions for Ames NACA 64A010 airfoil for several freestream Mach numbers.**

case of unsteady flow about a single mean operating condition. To test the method, we computed the unsteady small-disturbance solution on the coarse grid for a Mach number  $M$  of 0.85 at 21 frequencies  $\omega$  equally spaced between 0.0 and 1.0, where here the frequency has been nondimensionalized by  $\sqrt{p_\infty/\rho_\infty}/c$  where  $c$  is the aerodynamic chord,  $p_\infty$  is the freestream pressure, and  $\rho_\infty$  is the freestream density. Because of the large computational cost of computing the eigenvalues of the complete CFD model, Eq. (15), we use a coarse grid for the present examples. In later examples, we use a fine mesh to reduce truncation error associated with a coarse grid. At each frequency, two solutions were computed, one for plunging motion of the airfoil and one for pitching motion about a point one-half chord upstream of the leading edge. The plunging motion solution at  $\omega = 0$  is zero, and is thus discarded, resulting in a total of 41 nontrivial solutions or snapshots. For negative frequencies, the small-disturbance solutions are simply complex conjugates of the solutions at the corresponding positive frequency. Thus, for no additional computational effort, we may include an additional 40 snapshots into the ensemble, i.e. for  $\omega = -0.05, -0.10, \dots, -1.0$ , for a total of 81 snapshots.

Having computed the snapshots, we next use the technique described in Section II.C to find the proper orthogonal decomposition basis vectors. Figure 3 shows the eigenvalues  $\lambda$  of the first 41 proper orthogonal decomposition vectors. One sees the vast majority of the “energy” is contained in the first 10 or so POD vectors, and the energy in the modes beyond mode 15 is insignificant.

Next, the POD vectors were used to compute the eigenvalues and eigenmodes of the aerodynamic system using the Ritz-like approach given by Eq. (28) in Section II.D. For the first case, we retained all 81 POD vectors in the analysis. The resulting eigenvalues are shown in Figure 4 along with the exact eigenvalues computed by solving the generalized eigenvalue problem formed from the original CFD model, Eq. (15). For the eigenvalues near the origin, the reduced-order model eigenvalues and the exact eigenvalues agree almost exactly. For the remaining eigenvalues,

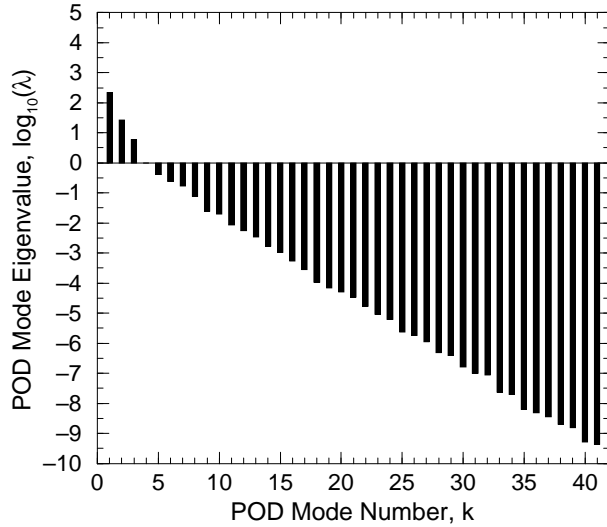


**Figure 3: Eigenvalues  $\lambda$  of the first 41 proper orthogonal decomposition vectors for small-disturbance flow about Ames NACA 64A010 airfoil ( $\alpha_0 = 0$ ,  $M = 0.85$ ) computed on coarse grid.**

the agreement is not as good, although the qualitative shape of the eigenvalue constellations are similar.

Next, we again computed the eigenvalues using the reduced-order model, but in this case retained the first 41 POD modes. These results are plotted in Figure 5. In this example, a few of the smallest eigenvalues are accurately computed, but many more are not. Nevertheless, the qualitative shape of the eigenvalue constellations are again similar. Similarly, Fig. 6 shows the eigenvalues computed using 21 of 81 POD modes.

Next, we used the POD basis vectors to construct the transfer function between the plunging and pitching motions of the airfoil and the resulting lift and moment. So, for example, to compute the transfer function between the pitching motion and lift, we prescribe a unit pitching motion at a complex frequency  $\omega$ . This motion defines the vector  $\mathbf{b}$  in Eq. (27). Equation (27) is then solved to determine  $\xi$ , the amount of each POD vector present in the unsteady small-disturbance solution. Then, using Eq. (24), the entire flow field is reconstructed from the basis vectors. The unsteady surface pressure is then integrated to obtain the unsteady lift.

Shown in Figure 7 shows the transfer function for three different values of  $\theta$  for a range of  $r$  where  $s = j\omega = r \exp(j\theta)$ . Shown is the “exact” transfer function computed using the small-disturbance CFD model, and also the present reduced-order model using 21 of the possible 81 POD vectors. The present reduced-order model is seen to be in excellent agreement with the full CFD model. A small difference between the two solutions is observed for  $\theta = 120^\circ$  for values of  $r$  above 0.2. Similarly, Fig. 8 shows the transfer function for a reduced-order model using just 6 of the possible 81 POD modes. Here the reduced-order model does not agree as well with the exact solution. However, the results are still quite acceptable for  $\theta = 90^\circ$ , especially considering the small number of POD vectors retained in

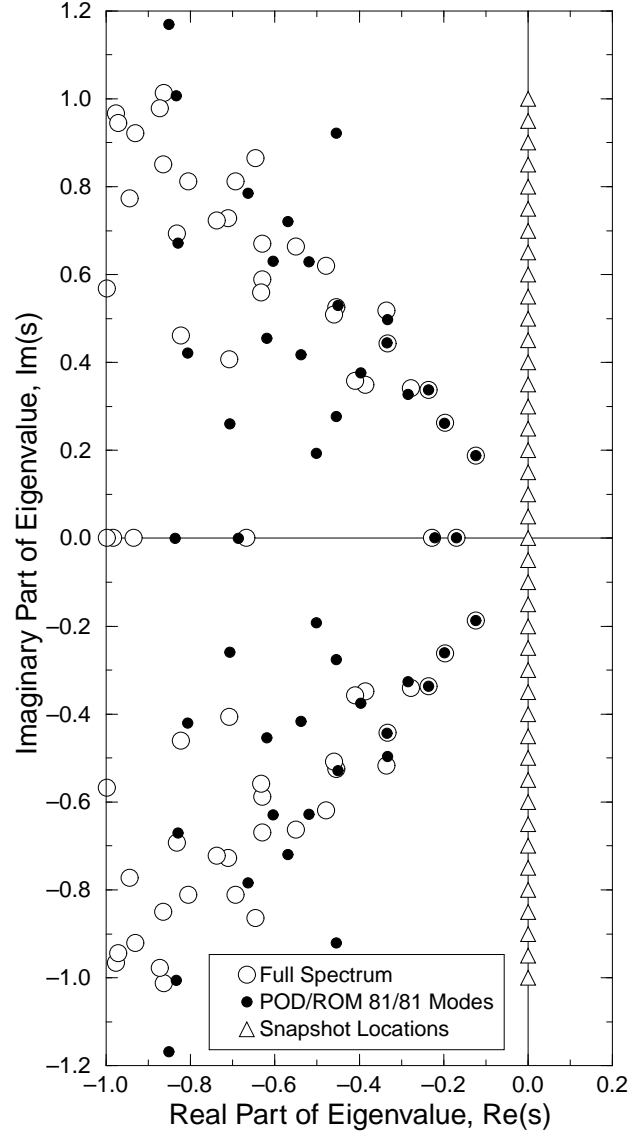


**Figure 4: Eigenspectrum of small-disturbance flow about Ames NACA 64A010 airfoil ( $\alpha_0 = 0$ ,  $M = 0.85$ ) computed on coarse grid. POD-ROM results computed using 81 of 81 POD Modes).**

the model.

Finally, by way of comparison, we plot in Fig. 9 the pitch to lift transfer function computed using a classical Padé approximation. Here we have used the matrix Padé approximant method described by Karpel [4]. The quality of the Padé approximation is about as good as the present reduced-order model using 6 POD vectors. However, the POD model is more general. If the problem is altered slightly, for example by changing the pitch axis, then new snapshots are not required; one may simply reuse the original POD vectors.

Next, we used the POD reduced-order modelling technique to compute the flutter boundary of the Ames NACA 64A010 airfoil. For this example, we used the fine computational grid ( $128 \times 32$  cells). We then computed a number of snapshots at each Mach number of interest. At each

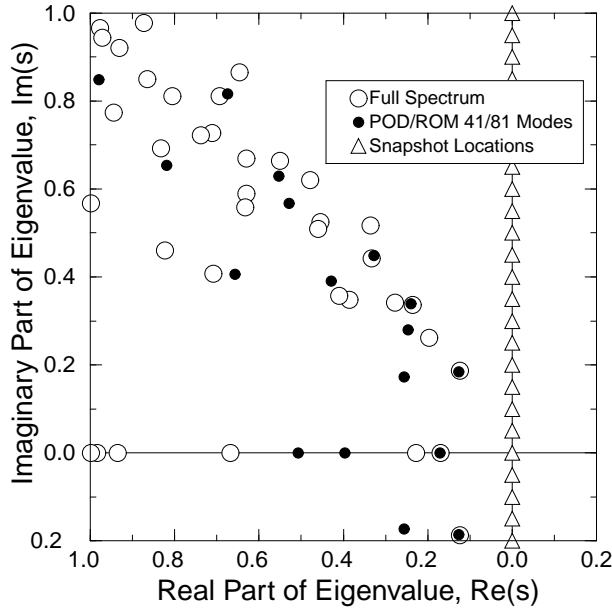


Figure 5: Eigenspectrum of small-disturbance flow about Ames NACA 64A010 airfoil ( $\alpha_0 = 0$ ,  $M = 0.85$ ) computed on coarse grid. POD/ROM results computed using 41 of 81 POD Modes).

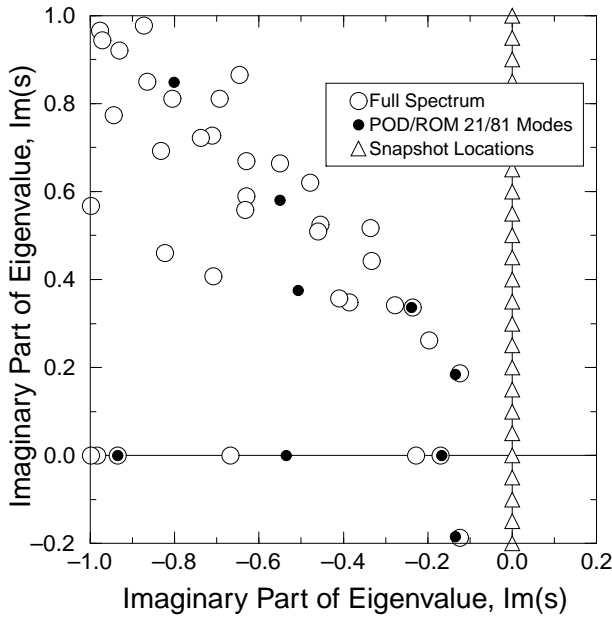


Figure 6: Eigenspectrum of small-disturbance flow about Ames NACA 64A010 airfoil ( $\alpha_0 = 0$ ,  $M = 0.85$ ) computed on coarse grid. POD/ROM results computed using 21 of 81 POD Modes).

Mach number, we computed the response at 11 nondimensional frequencies  $\omega$  equally spaced between 0.0 and 1.0. At each frequency, two solutions were computed, one for plunging motion and one for pitching motion. Again, noting that the plunging motion solution is zero for zero frequency and that solutions for negative frequencies are complex conjugates of the solutions at positive frequencies, we

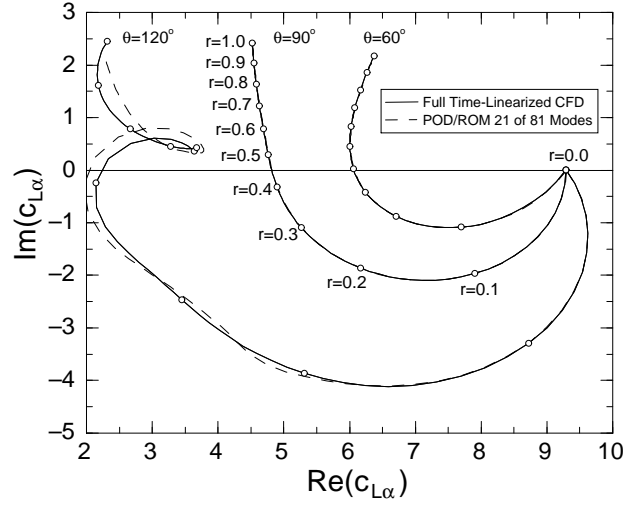


Figure 7: Unsteady lift due to pitching motion of Ames NACA 64A010 airfoil computed with 21 of 81 POD modes ( $\alpha_0 = 0$ ,  $M = 0.85$ ).

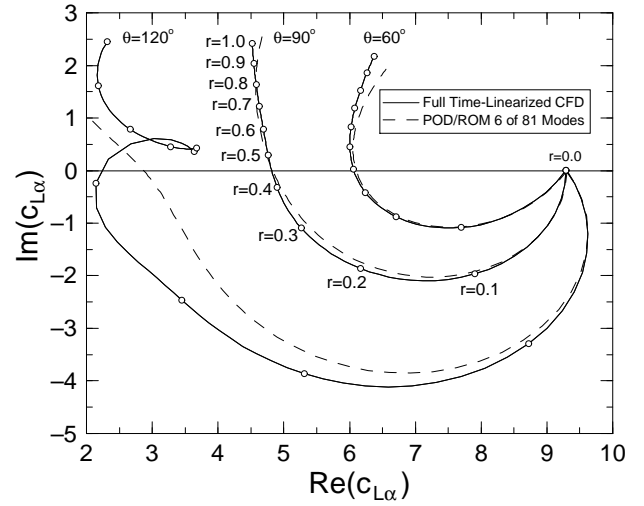


Figure 8: Unsteady lift due to pitching motion of Ames NACA 64A010 airfoil computed with 6 of 81 POD modes ( $\alpha_0 = 0$ ,  $M = 0.85$ ).

obtain a total of 41 snapshots.

Figure 10 shows the root locus of the (aeroelastic) eigenvalues of the reduced-order aeroelastic model given by Eq. (37) at several steady flow Mach numbers as the reduced velocity  $V = U_\infty / (\sqrt{\mu \omega_\alpha b})$  is varied, where  $\mu$  is the mass ratio,  $b$  is the semi-chord, and  $\omega_\alpha = \sqrt{k_\alpha / m}$ . As the reduced velocity is increased, one of the eigenvalues becomes unstable (positive real part). At  $M = 0.80$  and  $0.85$ , the mode which goes unstable as the reduced velocity is increased is the predominately plunging mode. For  $M = 0.9$ , the unstable mode is the pitching mode.

Figure 11 shows the reduced velocity at which one of the two aeroelastic modes becomes neutrally stable as a function of Mach number. Shown are the results predicted using three reduced-order models, with 11, 21, and 41 POD modes, respectively. All are in good agreement with one another; the 21 and 41-mode models are virtually indis-

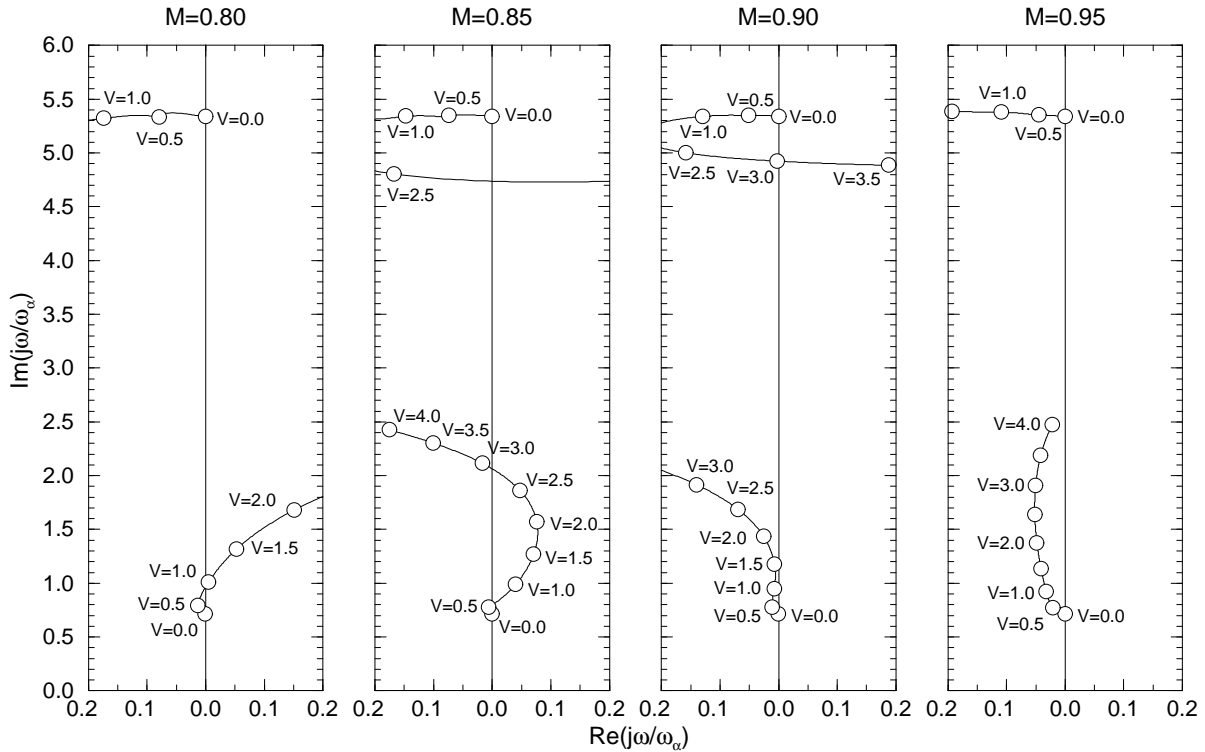


Figure 10: Aeroelastic eigenvalues of Ames NACA 64A010 airfoil for various Mach numbers computed using reduced-order models.

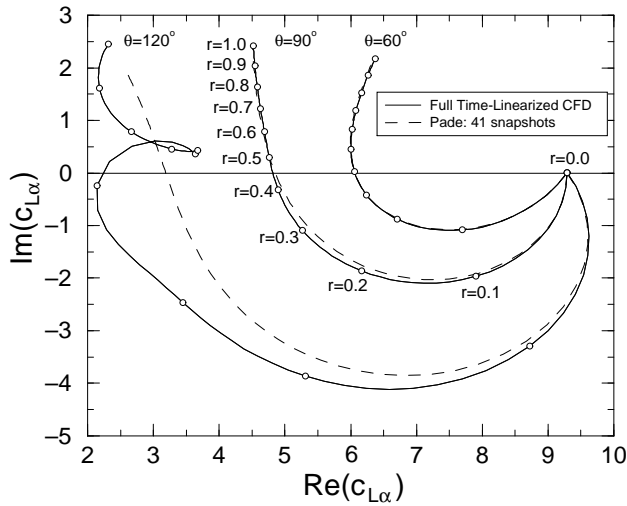


Figure 9: Unsteady lift due to pitching motion of Ames NACA 64A010 airfoil computed with matrix Padé approximant ( $\alpha_0 = 0$ ,  $M = 0.85$ ).

tinguishable. Also shown for comparison in Fig. 11 are flutter speeds predicted using transonic small disturbance (TSD) theories of Edwards [29] and Isogai [30], and the time-linearized full potential theory of Ehlers & Weatherill [31]. The present method and the potential theories all show the classic transonic dip in flutter speed, although the rise in flutter speed after the dip occurs at a slightly lower Mach number in the potential theories.

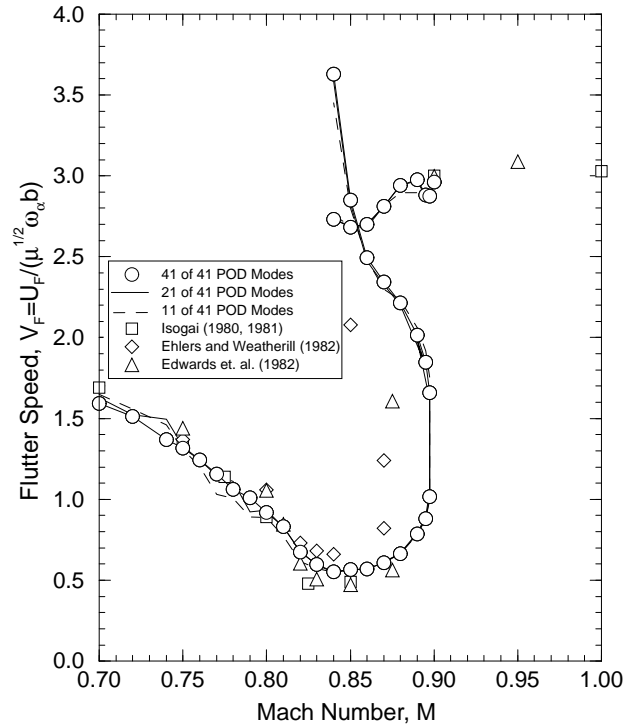
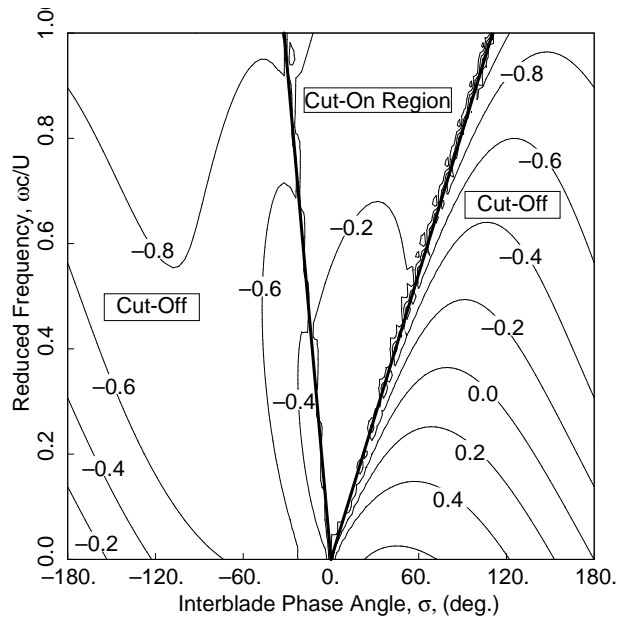


Figure 11: Flutter speed of Ames NACA 64A010 airfoil for various Mach numbers computed using reduced-order models.

## B. Turbomachinery Cascade Model Problem

The next case we consider is that of a cascade of flat-plate two-dimensional airfoils with steady flow Mach number of



**Figure 12: Imaginary part of aerodynamic moment due to pitching of cascade of airfoils computed using Whitehead's [32] LINSUB analysis.  $M = 0.7$ ,  $G = 1$ ,  $\Theta = 45^\circ$**

0.7. For this example, the gap-to-chord ratio  $G$  is 1.0, and the stagger angle  $\Theta$  is  $45^\circ$ . Because the mass ratio  $\mu$  of turbomachinery blading is very large, the flutter mechanism is not usually the frequency-coalescence type observed in aircraft wings. The unsteady aerodynamic forces do not significantly alter the natural frequency or mode shape of the airfoil's vibration. However, the unsteady aerodynamic forces can provide a small amount of positive or negative aerodynamic damping. Whenever the aerodynamic damping is negative, the airfoil will flutter (in the absence of structural damping). Shown in Fig. 12 is the imaginary component of the unsteady aerodynamic moment due to pitching as a function of interblade phase angle and reduced frequency  $\omega c/U_\infty$  computed using Whitehead's [32] semi-analytical analysis (LINSUB). The dark lines demark the boundary between sub-resonant and super-resonant flow conditions. Generally, the solution will change abruptly as crosses these boundaries. Using Whitehead's sign convention, whenever the imaginary part of the moment is positive, the aerodynamic damping is negative, and the cascade will flutter. One observes that there is a range of interblade phase angles between  $0^\circ$  and  $180^\circ$  for which the cascade will flutter at low reduced frequencies (high reduced velocities).

Next, we constructed a reduced-order aerodynamic model for this case using the POD technique applied to a cascade version of the small-disturbance flow solver described in Sec. II.B. We computed snapshots at a combination of six reduced frequencies ( $\omega c/U_\infty = 0.0, 0.2, 0.4, 0.6, 0.8, 1.0$ ) and six interblade phase angles ( $\sigma = -180^\circ, -120^\circ, -60^\circ, 0^\circ, 60^\circ, 120^\circ$ ) for a total of 36 snapshots. The POD modes of this set of solutions were computed, and the dominant 18 modes were used to construct a single reduced-order model valid over a range of interblade phase angles and frequencies. The imaginary

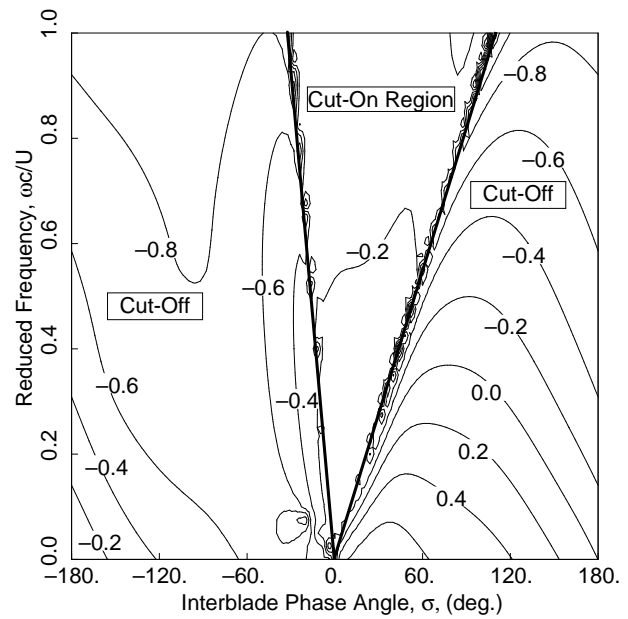


**Figure 13: Imaginary part of aerodynamic moment due to pitching of cascade of airfoils computed using POD/ROM technique with 18 of 31 POD modes.  $M = 0.7$ ,  $G = 1$ ,  $\Theta = 45^\circ$**

part of the unsteady pitching moment computed using this approach is shown in Fig. 13, and is seen to be in good agreement with the semi-analytical solution of Whitehead shown in Fig. 12. The overall good agreement is especially remarkable considering that only 18 aerodynamic state variables are required to model the unsteady flow over a significant range of interblade phase angles and reduced frequencies.

#### IV. Summary and Discussion

In this paper, we have described a method for constructing low-order reduced-order models using the proper orthogonal decomposition technique in conjunction with a time-linearized (frequency-domain) flow solver. The method has been applied to two model flow problems, i.e., unsteady transonic flow about an isolated airfoil, and subsonic flow through a cascade of flat-plate airfoils. In both cases, we were able to construct accurate low-order model of the unsteady flow; typical reduced-order models require on the order of 20 or fewer aerodynamic states. Additionally, we have shown how to couple the reduced-order aerodynamic model to a structural dynamic model to obtain a reduced-order aeroelastic model.

The major computational cost is the computation of the unsteady small-disturbance solutions (snapshots) from which the POD vectors are extracted. However, once the POD vectors have been found, the cost of constructing and solving the reduced-order model is negligible, allowing one to quickly perform parametric studies. Additionally, unlike a conventional V-g analysis, the resulting eigenvalues are meaningful at all flow velocities above and below the flutter velocity, i.e. for non-neutrally stable solutions. Furthermore, the form of the resulting reduced-order model, with its small number of degrees of freedom, is ideally

sued for use in active control applications. While in the present paper we have applied the technique to only two-dimensional flows, the method is general, and is equally applicable to three-dimensional unsteady aerodynamic and aeroelastic problems.

### Acknowledgments

This work was funded through a GUIde Consortium subcontract from Carnegie Mellon University, Subcontract No. 537032-57209, with original funding provided through NASA Lewis Research Center, Contract No. NAS3-27735; Jerry Griffin and Anatole Kurkov are the respective technical monitors. This work is part of NASA's Advanced Subsonic Technology (AST) program managed by Peter Batteredon and John Rohde. Additional funding was provided by Air Force Office of Scientific Research Grant No. F49620-97-1-0063, with Major Brian Sanders serving as program officer.

### References

- [1] Jones, R. T., "The Unsteady Lift of a Wing of Finite Aspect Ratio," NACA Report 681, 1941.
- [2] Vepa, R., "On the Use of Padé Approximates to Represent Unsteady Aerodynamic Loads for Arbitrarily Small Motions of Wings," AIAA Paper 76-17, Jan. 1976.
- [3] Edwards, J. W., "Applications of Laplace Transform Methods to Airfoil Motion and Stability Calculations," AIAA Paper 79-0772, April 1979.
- [4] Karpel, M., "Design for Active Flutter Suppression and Gust Alleviation Using State-Space Aeroelastic Modeling," *Journal of Aircraft*, Vol. 19, No. 3, 1982, pp. 221-227.
- [5] Hall, K. C., "Eigenanalysis of Unsteady Flows About Airfoils, Cascades, and Wings," *AIAA Journal*, Vol. 32, No. 12, 1994, pp. 2426-2432.
- [6] Hall, K. C., Florea, R., and Lanzkron, P. J., "A Reduced Order Model of Unsteady Flows in Turbomachinery," *Journal of Turbomachinery*, Vol. 117, No. 3 1995, pp. 375-383.
- [7] Florea, R., and Hall, K. C., "Eigenmode Analysis of Unsteady Flows about Airfoils," *Journal of Computational Physics*, Vol. 147, Dec. 1998, pp. 568-593.
- [8] Romanowski, M. C. and Dowell, E. H., "Reduced Order Euler Equations for Unsteady Aerodynamic Flows: Numerical Techniques," AIAA Paper 96-0528, Jan. 1996.
- [9] Dowell, E. H., Hall, K. C., and Romanowski, M. C., "Eigenmode Analysis in Unsteady Aerodynamics: Reduced Order Models," *Applied Mechanics Review*, Vol. 50, No. 6, 1997, pp. 371-386.
- [10] Loève, M., *Probability Theory*, D. Van Nostrand Company, Inc., New York, 1955.
- [11] Lumley, J. L., "The Structures of Inhomogeneous Turbulent Flow," in *Atmospheric Turbulence and Radio Wave Propagation*, edited by A. M. Yaglom and V. I. Tatarski, Nauka, Moscow, 1967, pp. 166-178.
- [12] Berkooz, G., Holmes, P., and Lumley, J. L., "The Proper Orthogonal Decomposition in the Analysis of Turbulent Flows," *Annual Review of Fluid Mechanics*, Vol. 25, 1993, pp. 539-575.
- [13] Poje, A. C. and Lumley, J. L., "A Model for Large-Scale Structures in Turbulent Shear Flows," *Journal of Fluid Mechanics*, Vol. 285, Feb. 25, 1995, pp. 349-369.
- [14] Sirovich, L., "Turbulence and the Dynamics of Coherent Structures. Part I: Coherent structures," *Quarterly of Applied Mathematics*, Vol. 45, No. 3, October 1987, pp. 561-571.
- [15] Sirovich, L., "Turbulence and the Dynamics of Coherent Structures. Part II: Symmetries and Transformations," *Quarterly of Applied Mathematics*, Vol. 45, No. 3, October 1987, pp. 573-582.
- [16] Sirovich, L., "Turbulence and the Dynamics of Coherent Structures. Part III: Dynamics and Scaling," *Quarterly of Applied Mathematics*, Vol. 45, No. 3, October 1987, pp. 583-590.
- [17] Moin, P. and Moser, R. D., "Characteristic-Eddy Decomposition of Turbulence in a Channel," *Journal of Fluid Mechanics*, Vol. 200, March 1989, pp. 471-509.
- [18] Rempher, D. and Fasel, H., "Evolution of Three-Dimensional Coherent Structures in a Flat-Plate Boundary Layer," *Journal of Fluid Mechanics*, Vol. 260, Feb. 10, 1994, pp. 351-375.
- [19] Rempher, D. and Fasel, H., "Dynamics of Three-Dimensional Coherent Structures in a Flat-Plate Boundary Layer," *Journal of Fluid Mechanics*, Vol. 275, Sept. 25, 1994, pp. 257-283.
- [20] Deane A. E., Kevrekidis, I. G., Karniadakis, G. E., and Orszag, S. A., "Low-Dimensional Models for Complex Geometry Flows: Application to Grooved Channels and Circular Cylinders," *Physics of Fluids A*, Vol. 3, No. 10, 1991, pp. 2337-2354.
- [21] Holmes, P., Lumley, J. L., and Berkooz, G., *Turbulence, Coherent Structures, Dynamical Systems and Symmetry*. Cambridge University Press, Cambridge, 1996.
- [22] Romanowski, M. C., "Reduced Order Unsteady Aerodynamic and Aeroelastic Models Using Karhunen-Loève Eigenmodes," AIAA Paper 96-3981, 1996.
- [23] Tang, K. Y., Graham, W. R., and Peraire J., "Active Flow Control Using a Reduced Order Model and Optimum Control," AIAA Paper 96-1946, 1996.
- [24] Kim, T., "Frequency-Domain Karhunen-Loève Method and Its Application to Linear Dynamic Systems," *AIAA Journal*, Vol. 36, No. 11, 1998, pp. 2117-2123.
- [25] Godunov, S. K., "A Finite Difference Method of the Numerical Computation of Discontinuous Solutions of the Equations of Fluid Dynamics," *Matematicheskii Sbornik*, Vol. 47, 1959, pp. 357-393.
- [26] Roe, P. L., "Approximate Riemann Solvers, Parameter Vectors, and Difference Schemes," *Journal of Computational Physics*, Vol. 43, 1981, pp. 357-372.
- [27] van Leer, B., "Towards the Ultimate Conservative Difference Scheme, II. Monotonicity and Conservation Combined in a Second-Order Scheme," *Journal of Computational Physics*, Vol. 14, 1974, pp. 361-376.
- [28] Bland, S. R., "AGARD Two-Dimensional Aeroelastic Configurations," AGARD AR-156, Neuilly-sur-Seine, France, August 1979.
- [29] Edwards, J. W., Bennett, R. M., Whitlow, W., Jr., and Seidel, D. A., "Time-Marching Transonic Flutter Solutions Including Angle-of-Attack Effects," *Journal of Aircraft*, Vol. 20, No. 11, 1983, pp. 899-906.

- [30] Isogai, K., "On the Transonic-Dip Mechanism of Flutter of Sweptback Wing," *AIAA Journal*, Vol. 17, No. 7, 1979, pp. 793–795.
- [31] Ehlers, F. E., and Weatherhill, W. H., "A Harmonic Analysis Method for Unsteady Transonic Flow and Its Application to the Flutter of Airfoils," NASA, CR-3537, May 1982.
- [32] Whitehead, D. S., "Classical Two-Dimensional Methods," *AGARD Manual on Aeroelasticity in Axial Flow Turbomachines. Vol. 1: Unsteady Turbomachinery Aerodynamics*, edited by M.F. Platzer and F.O. Carta, AGARD, Neuilly-sur-Seine, France, AGARD-AG-298 Vol. 1, March 1987, Chap. 3.